Improving the photocatalytic properties of anatase TiO_2 (101) surface by co-doping with Cu and N: Ab initio study

V. Koteski,* J. Belošević-Čavor, A. Umićević, V. Ivanovski, and D. Toprek

Vinča Institute of Nuclear Sciences, University of Belgrade, Serbia

E-mail: vkotes@vin.bg.ac.rs

Abstract

Substitutionally and interstitially Cu/N co-doped anatase TiO_2 (101) surface is investigated by using density functional theory (DFT) calculations. The results suggest improved visible light photocatalytic activity over undoped anatase TiO_2. Sizable lattice relaxation around the dopants is observed, followed by a formation of N-O bond. Depending on the local arrangement of atoms, localized states above the valence band maximum, deep into the band gap, and below the conduction band minimum are found. In addition, our calculation also predict band gap narrowing. The hybridization of the Cu 3d and N 2p states within the band gap and the other electronic and optical properties suggest a synergistic effect of the dopants in the enhancement of the visible light absorption on the (101) anatase surface.

Introduction

Because of its low cost, non-toxicity, and great stability under irradiation, TiO_2 is a promising material for photocatalytic water splitting and degradation of environmentally harmful

pollution.[1,2] While highly efficient under ultraviolet irradiation, it is not active in the visible light region. The band gaps of the rutile and anatase polymorphs of TiO_2 are 3.3 and 3.2 eV, respectively,[3,4] which is too large for absorption of visible photons. In order to be able to improve the photocatalytic activity of TiO_2 under visible light irradiation, it is therefore necessary to shift the absorption edge toward longer wavelengths.

One of the methods of modifying the properties of semiconducting materials is introducing suitable impurities. Modification of the surface of TiO_2 by foreign atom doping is a promising approach in improving the photocatalytic performance. The other line of research is synthesizing efficient nanocomposite materials.[5] Dopant atoms in TiO_2 can cause band gap narrowing, which is beneficial for enhancing the photocatalytic reactions efficiency of this material. Typically, transition metals like Cr, Mn, Fe, Ag, V, and Cu[6–14] and non-metals like C, N, S, Si, and F[15–20] are used. Additional limiting factor for photocatalytic applications is the relatively short life of the excited electron-hole pairs in TiO_2. Impurity atoms can also create new defect complexes and introduce deep defect levels that may act as trapping centers, favoring charge separation.[21,22]

Recent research studies suggest that co-doping by non-metals in combination with transition metals has a strong synergistic effect in enhancing the visible light photocatalytic activity. For example, DFT calculations confirm the redshift of the optical absorption edge in Fe/Si co-doped TiO_2 anatase.[9] Another DFT study of W and N codoped TiO_2[23] also confirmed significant narrowing of the band gap of both anatase and rutile.

Nitrogen doping of TiO_2 is a known strategy to produce material responsive in the visible region.[24,25] Doping with N and other anions (C,S) can be used to model the shape of the density of states at the top of the valence band. In N-monodoped bulk anatase, the N 2p states are found above the valence band maximum.[11,26]

Copper is one of the transition metals impurities used for doping of TiO_2 anatase because it has the ability to improve the absorption in the visible light region.[27] The incorporation of copper into TiO_2 anatase leads to appearance of Cu $3d$ states near the top of the valence

band, while substitutional doping of Cu is also predicted to shift the optical absorption spectra to the long wavelength region.[10] In Cu/S co-doped bulk TiO_2 anatase, the impurity energy levels are found to be predominantly of Cu 3d and S 3p types.[28]

The characterization of Cu-doped anatase nanoparticles[12] has shown band gap narrowing in the doped nanostructures and increased photocatalytic activity for the system with 0.05 at. % of Cu. Increased photocatalytic activity in the visible spectrum was also observed in Cu(II)-grafted TiO_2.[14] A recent DFT study of substitutional copper dopants on the (101) anatase surface has predicted the appearance of inter-bandgap defect states, which are considered responsible for the improved visible-light photoactivity in anatase.[29]

The ability of copper to form clusters on top of the (101) surface of anatase has been investigated in a recent DFT study.[13] The authors found that Cu plays a role in the separation of the photogenerated electrons and holes, and should enhance the photo-response of TiO_2.

Enhanced absorption in the visible light region and a red shift in the band gap transition in a N/Cu co-doped TiO_2 nanoparticles have been reported experimentally.[30–34] In the Cu/N codoped anatase thin films hindered excitation recombination was detected.[35] Cu, N, and Cu/N doping of bulk anatase[36] was also studied by using DFT. The bulk calculations have shown that the photocatalytic activity of the co-doped system is higher than the corresponding undoped or mono-doped systems.

In this work we investigate the impact of copper and nitrogen co-doping on the structural, electronic, and optical properties of (101) anatase surface. Anatase was chosen as the more efficient form of TiO_2 for photocatalytic applications.[37] The (101) surface of anatase is predicted to be the most stable[38] and as such represents the largest portion of the exposed surface area in nanostructures. To the best of our knowledge this is the first ab-initio study to consider anatase surface co-doping with these two important elements. We calculate the defect formation energy of several characteristic substitutional and interstitial configurations of Cu and N. We focus on the defect complexes that appear in the topmost layers of the (101)

surface of TiO_2 anatase. We show that the incorporation of Cu and N into TiO_2 anatase can increase the photocatalytic activity in the visible light region regardless of the actual local arrangement of dopant atoms. The energetically most favorable defect configuration in this system is found to be an interstitial nitrogen or nitrogen adsorbed to the surface close to an oxygen atom in combination with a substitutional copper.

DFT Calculations

Our calculations are based on the density functional theory (DFT) implemented in the grid-based projector-augmented wave program GPAW.[39–42] To describe the electronic exchange and correlation effects we used the PBE functional.[43] Approaches that employ semi-empirical corrections like the DFT+U corrections[44] give values of the band gaps much closer to the experimental result, but sometimes at the expense of structural properties.[45] The energy cut-off in our calculations was set to 350 eV. For the calculations of the bulk unit cell of TiO_2 anatase, we used a MonkhorstPack grid of 21×21×9 k-points.

TiO_2 anatase crystallizes in a tetragonal body centered unit cell (space group $I4_1/amd$). The primitive unit cell of anatase contains 4 Ti and 8 O atoms. They are at Wyckoff positions $4a$ (0, 0, 0) for Ti and $8e$ (0, 0, 0.208) for O.

The experimental lattice parameters of TiO_2 anatase, as determined with neutron diffraction at 15K, are a=3.782 and c=9.502 Å,[46] while the u parameter related to the z coordinate of the oxygen atom is 0.208. Our calculated lattice parameters of a=3.743 Å, c=9.456 Å, and u=0.208 are all within 1 % of their corresponding experimental values.

The (101) surface of TiO_2 anatase is known to have the lowest surface energy.[38,47] To test this for our theoretical approach, we have calculated the surface energy of three low-energy facets of TiO_2 anatase: (100), (001), and (101). The surface energy of the (101) facet of TiO_2 anatase after atomic relaxation was found to be 0.59 J/m^2. The surface energy of the second most stable (100) facet was 0.87 J/m^2, while the relaxed (001) surface was calcualted to

have a surface energy of 1.11 J/m^2. The values of the calculated surface energies and their relative order agree well with the previous calcualtions.[48,49]

Given the above results, we have constructed our surface unit cell to be with 101 termination. We modeled this system by using a 3×1 rectangular surface cell with parameters obtained from the optimized bulk geometry(10.17 × 11.23 Å). A slab of 108 atoms was periodically repeated in x and y direction and a vacuum space of 10 Å thickness was added along the surface normal (Fig. 1). In this geometry, the outermost oxygen atom is two-fold coordinated. The next layer consists of 5-fold coordinated Ti atoms (Ti^5), followed by a 3-fold coordinated O atoms, and a 6-fold coordinated Ti atoms (Ti^6).

Given the size of the supercell, for all slab calculations we used only the Γ point, with a grid spacing of 0.2 Å.

Keeping the atoms in bottom-most TiO_2 layer in the undoped system fixed (a total of 12 Ti and 24 O atoms), we relaxed the positions of the remaining atoms in the supercell. We then introduced the dopant atoms and further relaxed the supercell.

The total energy in our calculations was converged to 10^{-5}eV/atom, whereas the criterion for force minimization was 0.03 eV/Å. The substitutional Cu/N co-doping was modeled by using one pair of host atoms replaced, which is situations corresponding to a concentration of ∼1.85 at. % of impurity atoms.

Defect Configurations and Formation Energy

We considered a variety of Cu and N surface and sub-surface positions, including co-doping on regular lattice sites and interstitial positions. In particular, we calculated the following configurations: (i) Cu_{Ti^5}-N_O: Cu substituting a 5-fold coordinated top layer Ti atom with N substituting on various O lattice sites, (ii) Cu_{Ti^6}-N_O: Cu substituting a 6-fold coordinated sub-surface Ti atom with a nitrogen atom substituting on O lattice sites, and (iii) Cu_{Ti}-N_i: N in the interstitial position with Cu substituting on Ti lattice sites in various layers.

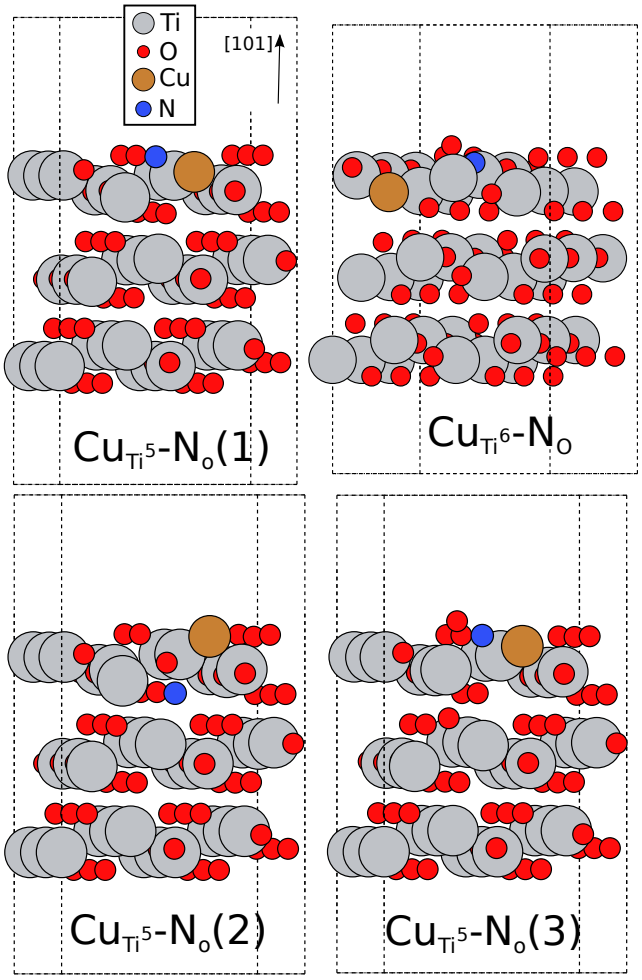

Figure 1: Atomic structures of TiO_2 anatase (101) surface after codoping with Cu and N substitutional atoms.

We also tried several antisite configurations (Cu substituting on O and N on Ti lattice site, or Cu interstitial and N substituting on Ti lattice site). After noticeable rearrangement of the dopants, most of these configurations transposed into one of the three former cases. The only exception was the configuration Cu_{Ti}-N_{ad} presented in Fig. 2, where the N dopant ended up on top of the slab. Incidentally, this was found to be the lowest formation energy structure among the investigated geometries.

The stability of the co-doped systems was estimated using the defect formation energy, E_f. For the cases (i) and (ii), E_f is defined as:

$$E_f = E_d - E_p - \frac{1}{2}\mu_{N_2} - \mu_{Cu} + \frac{1}{2}\mu_{O_2} + \mu_{Ti}, \quad (1)$$

where E_d is the DFT total energy of the doped supercell, E_p is the energy of the supercell without impurities, μ_{Cu} and μ_{Ti} are the total energies of the bulk Cu and Ti metals per atom, and μ_{N_2} and μ_{O_2} are the DFT total energies of nitrogen and oxygen molecules.

For the case (iii), we used this slightly modified expression:

$$E_f = E_d - E_p - \frac{1}{2}\mu_{N_2} - \mu_{Cu} + \mu_{Ti}. \quad (2)$$

Figure 1 depicts several typical substitutional configurations obtained after ionic relaxation: Cu_{Ti^5}-$N_O(1)$, Cu_{Ti^5}-$N_O(2)$, and Cu_{Ti^5}-$N_O(3)$ with Cu replacing a five-fold coordinated Ti atom and Cu_{Ti^6}-N_O where Cu substitutes a six-fold coordinated Ti atom.

Cu_{Ti^5}-$N_O(1)$ is the least distorted configuration with respect to the slab's equilibrium geometry. At the same time, its formation energy (see Table 1) is the highest among the structures presented here. In the other cases, the substitutional N is subject to a sizable lattice relaxation. As a result, a short bond (1.31 - 1.35 Å) with a neigboring oxygen atom is built. By comparison, the shortest O-O bond length in pure TiO_2 anatase is 2.47 Å. At the same time, Cu is displaced from the original Ti lattice site position. This local lattice deformation seems to favor the stabilization of the defects by lowering the energy of the

system.

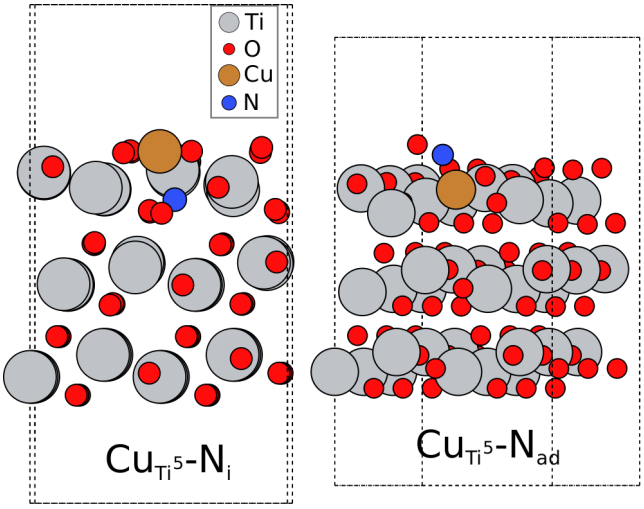

Figure 2: Lowest formation energy configurations of TiO_2 anatase (101) surface codoped with Cu and N.

The structures with the lowest and second lowest formation energy, Cu_{Ti}-N_{ad} and Cu_{Ti}-N_i, respectively, are shown in Fig. 2. Cu_{Ti}-N_i is obtained starting from an interstitial N and substitutional Cu configuration. The structure Cu_{Ti}-N_{ad} is the end result of geometry optimization of antisite (N on Ti) and interstitial Cu initial configuration. Again we see the same motif, a short N-O bond accompanied with a more or less displaced Cu_{Ti}.

Here, the attraction between N and O is even stronger, and the N-O distance is shorter (1.21 Å for Cu_{Ti}-N_{ad} and 1.24 Å for Cu_{Ti}-N_i). These values are not far from the molecular nitric oxide equilibrium bond length of 1.15 Å.[50] Except for Cu_{Ti^5}-$N_O(1)$, in all the other atomic structures this strong attraction of N toward a neighboring O appears to be a characteristic pattern.

Electronic Structure

Further insight into the electronic structure of the Cu/N co-doped anatase (101) surface can be obtained if we consider the total density of states (DOS) and partial density of states (PDOS) (Fig. 3 and Fig. 4, respectively). Within the PBE formalism of the DFT

Table 1: Defect formation energy (E_f) and bond lengths (d) for different relaxed configurations of TiO_2 anatase surface codoped with Cu and N.

	E_f(eV)	d_{N-Cu}(Å)	d_{N-Ti}(Å)	d_{N-O}(Å)	d_{Cu-O}(Å)
Cu_{Ti^5}-N_O (1)	13.4	1.76	2.16	2.44 2.81 2.88	1.93 1.94 2.14
Cu_{Ti^6}-N_O	12.2	4.03	2.10 2.14 2.39	1.35 2.59 2.81 2.85	1.93 2.03 2.22
Cu_{Ti^5}-N_O (2)	12.0	2.75	2.19 2.26	1.31 2.79 2.72	2.03 2.10 2.12
Cu_{Ti^5}-N_O (3)	11.4	1.85	2.06	1.31 2.71 2.72	1.93 208 2.09
Cu_{Ti}-N_i	10.4	2.03	2.73	1.24 1.85 2.66 2.84	1.80 1.85 2.81 2.84
Cu_{Ti}-N_{ad}	8.9	1.92	3.46	1.21 1.94	1.93 2.18 2.72 2.81

implemented here, the band gaps of bulk anatase and anatase 101 surface are 2.05 eV and 1.89 eV, respectively. The result is consistent with previous calculations based on this approximation[51,52] and is a consequence of the shortcomings of the DFT to accurately describe the localized Ti 3d states. If compared to the surface gap, the calculated bulk band gap is smaller, which is expected as a result of additional gap states due to dangling bonds on the anatase surface.[53]

All Cu/N co-doped atomic systems exhibit band gaps smaller than the pure surface. This narrowing of the band gap can lead to shift of the optical absorption toward the visible light spectrum, which is indeed confirmed by our calculations of the absorption spectra (see below).

The DOS shows the appearance of small peaks at and above the top of the valence band (VB), within the band gap, and close to the bottom of the conduction band (CB). These peaks, which are not present in the pure, undoped surface, are a direct consequence of Cu and N impurity states. The main contribution of a mono-doped substitutional Cu to the DOS comes from its 3d states, which are positioned at the VB maximum and deeper in the band gap. Similarly for mono-doped substitutional and interstitial N, the main contributions come from the N 2p states positioned at the top and slightly above the VB. Because of this, nitrogen doping of TiO_2 anatase has already been proven to be a great method for narrowing of the band-gap and improving the photocatalytic activity by both x-ray photoemission spectroscopy and first-principles calculations.[11,24]

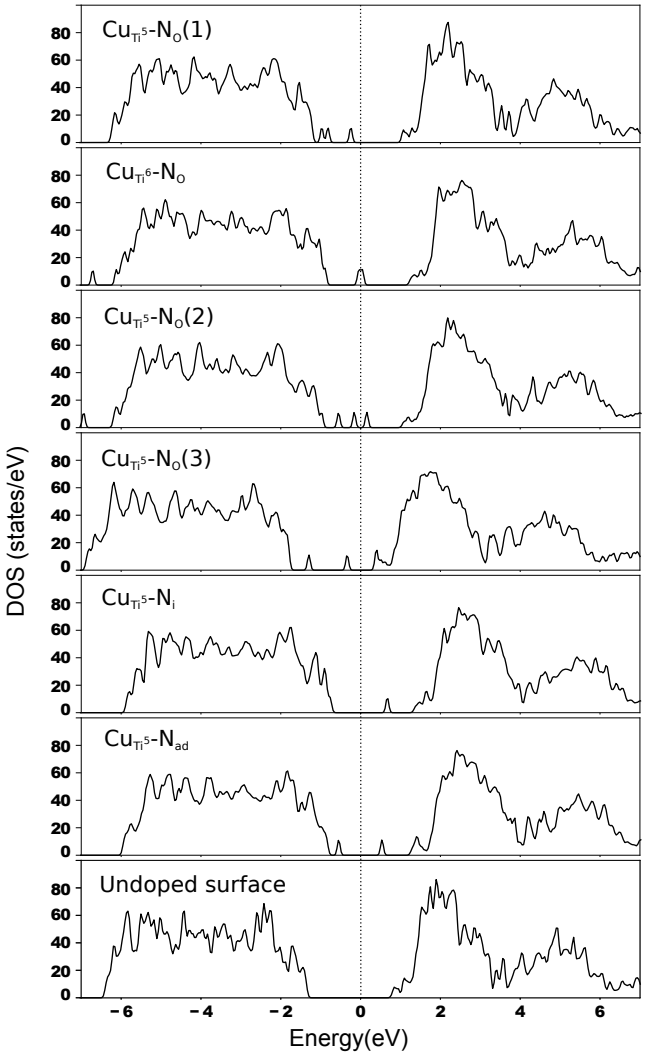

Figure 3: Total density of states for the pure and codoped 108-atom TiO_2 surface. The Fermi energy, depicted as dotted line, is taken as a reference level.

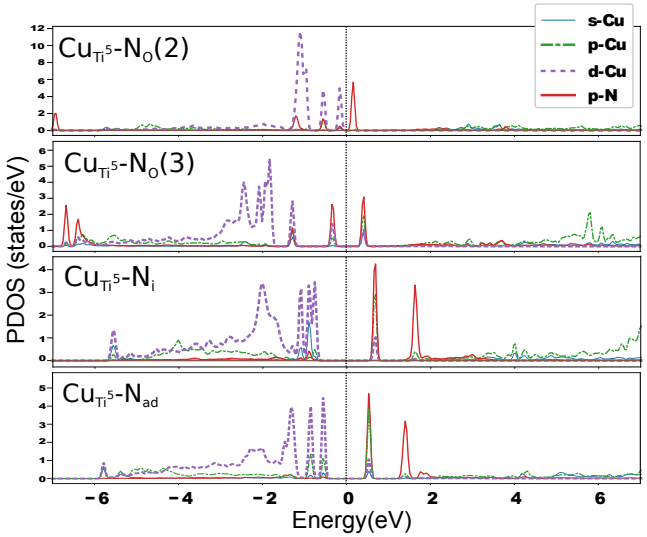

Figure 4: Cu and N partial density of states in a co-doped 108-atom TiO_2 surface. The Fermi energy, depicted as dotted line, is taken as a reference level.

Moreover, the simultaneous doping with both Cu and N seems to enhance the complexity in the band gap by altering the defect levels and via hybridization. Depending on the defect system, this can be seen in the PDOS of the co-doped anatase (101) surface presented in Fig. 4. For example, the configurations Cu_{Ti^5}-N_O (3), Cu_{Ti}-N_{ad} and Cu_{Ti}-N_i have their N 2p defect levels and to some degree their Cu 3d levels pushed deeper into the band gap and closer to the top of the CB. Furthermore, these three lowest formation energy defects exibit a noticeable hybridization between the Cu 3d and N 2p states, as can be seen by the varying degree of overlap between the Cu and N states. We also see that the higher the defect lies in the band gap, the smaller the contribution of the Cu d states and more dominant the contribution of the N p states.

To evaluate the suitability of the Cu-N codoped anatase as visible light photocatalyst and to explain its experimentally observed enhanced photocatalytic activity,[34] we will make an attempt to correlate our obtained results for electronic structure with the electronic structure that an efficient photocatalyst is supposed to have. First and foremost, for the efficient use of TiO_2 for photocatalytic water splitting, it is necessary to find a dopant pair which narrows the band gap in order to shift the absorption edge to the visible light region, but at the same

time does not lower the conduction band minimum, as the reduction potential level of water is just below the CBM of TiO_2.[54]

The narrowing of the band gap for almost all the investigated Cu/N codoped configurations (the only exception is energetically unfavored Cu_{Ti^5}-N_O (3)) due to the rise of VB maximum and the formation of intermediate states, while leaving the conduction band almost unchanged, qualify this system to be an efficient material for the photocatalytic water splitting. Besides, in order to avoid the creation of electron-hole recombination centers, which reduce the lifetime of the photo-induced charge carriers and thus lead to a decrease of photocatalytic activity, ideal photocatalyst should have band gap with no additional states inside.[55,56] Namely, the creation of the impurity states at the mid-band energy level (EMB), defined as half of the energy difference of the top energy level of the VB and the bottom energy level of the CB, will maximize the recombination rate of the electron-hole pairs, causing minimal photocatalytic efficiency.

In the cases studied here, for the energetically preferential doping structures (Cu_{Ti}-N_{ad} and Cu_{Ti}-N_i) the impurity states created inside the band gap are located in the lower and top third of the band gap. Hence the life time of the charge carriers is reduced, but does not reach its minimum as in the case of impurity states at EMB. In total, Cu/N codoping of TiO_2 anatase (101) surface, causes a redshift in the absorption and introduces band gap states that do not cause the recombination rate to maximize, and therefore conserve a reasonable photocatalytic efficiency, which makes it a suitable material for visible light photocatalyst. The obtained results are in line with the experimental ones, which evidenced that Cu/N codoping caused an increase of both the mean lifetime and trapping rate of defects at the nanocolumn surface in the anatase network,[35] along with the enhancement of the photocatalytic efficiency.[34]

Optical Absorption

We used linear response calculations[41] within the adiabatic local density approximation to determine the optical absorption of our systems. The absorption spectra were calculated using the time-dependent density functional theory (TDDFT)[57] from the density response function. More details about the calculation can be found in Ref.[58]

The coefficient of optical absorption as a function of wavelength of the pure and Cu/N co-doped anatase (101) surface is presented in Fig. 5. We have calculated two sets of spectra, for light polarized in the x direction (perpendicular to the surface normal) and for light polarized along the z direction (parallel to the surface normal). For all Cu/N local atomic arrangements considered here, there is an improvement of the optical absorption in the visible region as compared to the pure TiO_2 anatase surface, although the main absorption peaks still occur in the UV range. The only exception can be seen for the defect complex between a substitutional Cu and interstitial N, Cu_{Ti}-N_i, which, in the region up to 500 nm, exhibits a weaker absorption for light photons polarized in z-direction than the undoped anatase surface. However, this particular local configuration has the largest absorption coefficient for light polarized in x-direction in the entire visible light region. When the light polarized in z-direction is concerned, Cu_{Ti^5}-N_O (2) and Cu_{Ti}-N_{ad} give the best visible light absorption and the longest extension of the absorption tail into the visible light region among the investigated configurations.

As far as the optical absorption in the UV region is conserned, our calculations indicate that it is only improved for light polarized perpendicularly to the surface. For light polarization in x-direction we observe a decline in the absorption coefficient below 350 nm.

Conclusion

We have calculated the local atomic structure, defect formation energy, DOS, and optical absorption coefficient of Cu and N impurities in the topmost layers of the anatase (101)

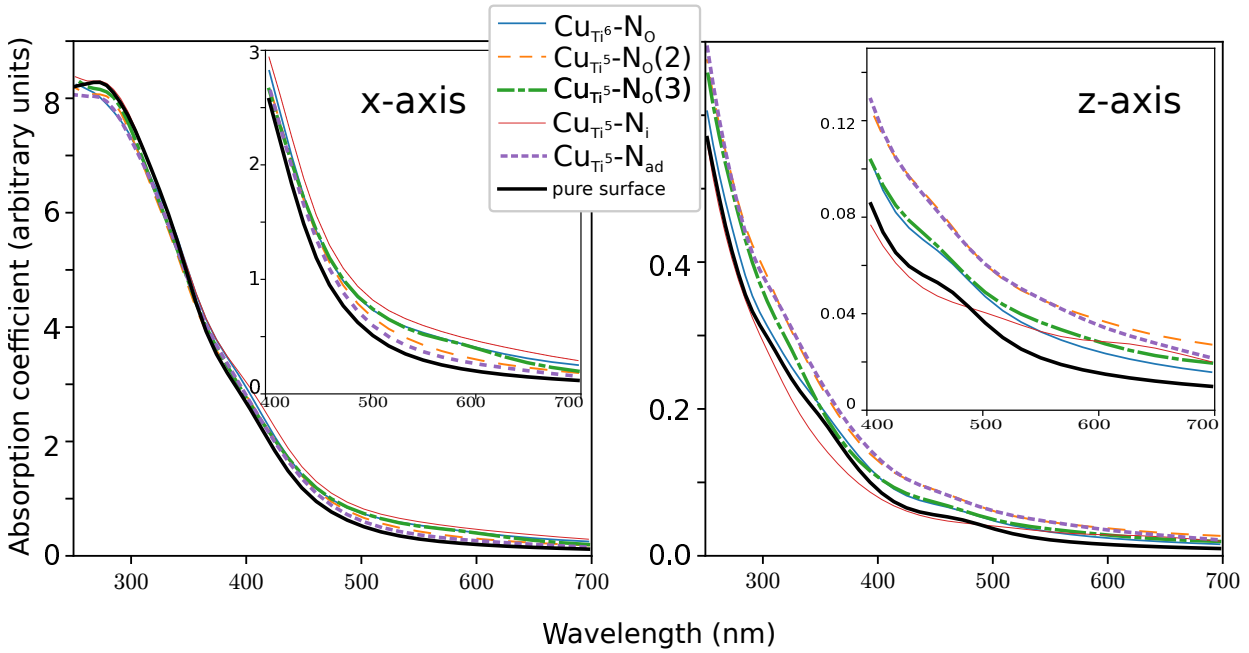

Figure 5: Polarization dependent optical absorption spectra of pure and Cu/N co-doped anatase (101) surface. The insets depict the visible light region.

surface. Based on their formation energy, the two most stable atomic arrangements are (i) interstitial nitrogen and (ii) nitrogen adsorbed to the surface, both in combination with a substitutional copper. Most of the local atomic arrangements are a result of sizable lattice relaxation after the introduction of the dopants. Another notable characteristic of this system is the strong tendency of N toward forming a relatively short N-O bond length with a neighboring O atom. Cu and N contribute to significant changes in the DOS of the anatase (101) surface, including the appearance of isolated states in the band gap. These states are found to be hybridized and, depending on the position in the band gap, have substantial Cu 3d and N 2p character. Our calculation confirm the experimentally determined enhancement of the visible light absorption of Cu/N co-doped TiO_2 anatase. All surface defect configurations considered in our work should be more or less effective for improving the visible light absorption, which could be important for photocatalytic water splitting and environmental applications of this material.

Acknowledgement

The financial support for this work was provided through the Projects No.171001 and 45018, financed by the Ministry of Education, Science and Technological Development of the Republic of Serbia.

References

References

(1) Abbasi, A.; Jahanbin Sardroodi, J. *Environ. Sci.: Nano* **2016**, *3*, 1153–1164.

(2) Abbasi, A.; Sardroodi, J. J. *Computational and Theoretical Chemistry* **2016**, *1095*, 15 – 28.

(3) Scanlon, D. O.; Dunnill, C. W.; Buckeridge, J.; Shevlin, S. A.; Logsdail, A. J.; Woodley, S. M.; Catlow, C. R. A.; Powell, M. J.; Palgrave, R. G.; Parkin, I. P.; Watson, G. W.; Keal, T. W.; Sherwood, P.; Walsh, A.; Sokol, A. A. *Nat Mater* **2013**, *12*, 798–801, Letter.

(4) Dette, C.; Prez-Osorio, M. A.; Kley, C. S.; Punke, P.; Patrick, C. E.; Jacobson, P.; Giustino, F.; Jung, S. J.; Kern, K. *Nano Letters* **2014**, *14*, 6533–6538, PMID: 25252265.

(5) Wen, M. Q.; Xiong, T.; Zang, Z. G.; Wei, W.; Tang, X. S.; Dong, F. *Opt. Express* **2016**, *24*, 10205–10212.

(6) Kollbek, K.; Szkudlarek, A.; Marzec, M.; Lyson-Sypien, B.; Cecot, M.; Bernasik, A.; Radecka, M.; Zakrzewska, K. *Applied Surface Science* **2016**, *380*, 73 – 82, Proceedings for International Conference on Surfaces, Coatings and Nanostructured Materials (NANOSMAT-10, Manchester, UK).

(7) Lu, L.; Xia, X.; Luo, J. K.; Shao, G. *Journal of Physics D: Applied Physics* **2012**, *45*, 485102.

(8) Li, Z.; Wang, X.; Jia, L.; Chi, B. *Journal of Molecular Structure* **2014**, *1061*, 160 – 165.

(9) Lin, Y.; Jiang, Z.; Zhu, C.; Hu, X.; Zhu, H.; Zhang, X.; Fan, J.; Lin, S. H. *International Journal of Hydrogen Energy* **2013**, *38*, 5209 – 5214.

(10) Guo, M.; Du, J. *Physica B: Condensed Matter* **2012**, *407*, 1003 – 1007.

(11) Belošević-Čavor, J.; Batalović, K.; Koteski, V.; Radaković, J.; Rangel, C. *International Journal of Hydrogen Energy* **2015**, *40*, 9696 – 9703.

(12) Christoforidis, K. C.; Fernandez-Garcia, M. *Catal. Sci. Technol.* **2016**, *6*, 1094–1105.

(13) Seriani, N.; Pinilla, C.; Crespo, Y. *The Journal of Physical Chemistry C* **2015**, *119*, 6696–6702.

(14) Nosaka, Y.; Takahashi, S.; Sakamoto, H.; Nosaka, A. Y. *The Journal of Physical Chemistry C* **2011**, *115*, 21283–21290.

(15) Di Valentin, C.; Pacchioni, G.; Selloni, A. *Chemistry of Materials* **2005**, *17*, 6656–6665.

(16) Umebayashi, T.; Yamaki, T.; Itoh, H.; Asai, K. *Applied Physics Letters* **2002**, *81*, 454–456.

(17) Yang, K.; Dai, Y.; Huang, B. *Chemical Physics Letters* **2008**, *456*, 71 – 75.

(18) Jia, L.; Wu, C.; Li, Y.; Han, S.; Li, Z.; Chi, B.; Pu, J.; Jian, L. *Applied Physics Letters* **2011**, *98*, 211903.

(19) Long, R.; English, N. J. *New Journal of Physics* **2012**, *14*, 053007.

(20) Lin, Y.; Jiang, Z.; Zhu, C.; Hu, X.; Zhang, X.; Zhu, H.; Fan, J.; Lin, S. H. *J. Mater. Chem. A* **2013**, *1*, 4516–4524.

(21) Neubert, S.; Mitoraj, D.; Shevlin, S. A.; Pulisova, P.; Heimann, M.; Du, Y.; Goh, G. K. L.; Pacia, M.; Kruczala, K.; Turner, S.; Macyk, W.; Guo, Z. X.; Hocking, R. K.; Beranek, R. *J. Mater. Chem. A* **2016**, *4*, 3127–3138.

(22) Najafian, A.; Rahimi, R.; Zargari, S.; Mahjoub-Moghaddas, M.; Nazemi, A. *Research on Chemical Intermediates* **2016**, *42*, 3441–3458.

(23) Long, R.; English, N. J. *Molecular Simulation* **2010**, *36*, 618–632.

(24) Asahi, R.; Morikawa, T.; Ohwaki, T.; Aoki, K.; Taga, Y. *Science* **2001**, *293*, 269–271.

(25) Nosaka, Y.; Matsushita, M.; Nishino, J.; Nosaka, A. *Science and Technology of Advanced Materials* **2005**, *6*, 143–148.

(26) Wenhui, X.; Xinguo, M.; Tong, W.; Zhiqi, H.; Huihu, W.; Chuyun, H. *Journal of Semiconductors* **2014**, *35*, 102002.

(27) Yu, H.; Irie, H.; Hashimoto, K. *Journal of the American Chemical Society* **2010**, *132*, 6898–6899, PMID: 20429504.

(28) Su, W.; Zhao, R.; Zheng, S. *Matéria (Rio de Janeiro)* **2016**, *21*, 599 – 605.

(29) Assadi, M. H. N.; Hanaor, D. A. *Applied Surface Science* **2016**, *387*, 682 – 689.

(30) Song, K.; Zhou, J.; Bao, J.; Feng, Y. *Journal of the American Ceramic Society* **2008**, *91*, 1369–1371.

(31) Reda, S.; Khairy, M.; Mousa, M. *Arabian Journal of Chemistry* **2017**, –.

(32) Tian, F.; Wu, Z.; Yan, Y.; Ye, B.-C.; Liu, D. *Nanoscale Research Letters* **2016**, *11*, 292.

(33) Wang, S.; Yang, X.; Jiang, Q.; Lian, J. *Materials Science in Semiconductor Processing* **2014**, *24*, 247 – 253.

(34) Jaiswal, R.; Bharambe, J.; Patel, N.; Dashora, A.; Kothari, D.; Miotello, A. *Applied Catalysis B: Environmental* **2015**, *168169*, 333 – 341.

(35) El Koura, Z.; Cazzanelli, M.; Bazzanella, N.; Patel, N.; Fernandes, R.; Arnaoutakis, G. E.; Gakamsky, A.; Dick, A.; Quaranta, A.; Miotello, A. *The Journal of Physical Chemistry C* **2016**, *120*, 12042–12050.

(36) Liu, Y.; Liang, W.; Zhang, W.; Zhang, J.; Han, P. *Solid State Communications* **2013**, *164*, 27 – 31.

(37) Luttrell, T.; Halpegamage, S.; Tao, J.; Kramer, A.; Sutter, E.; Batzill, M. *Scientific Reports* **2014**, *4*, 4043 EP –, Article.

(38) Labat, F.; Baranek, P.; Adamo, C. *Journal of Chemical Theory and Computation* **2008**, *4*, 341–352, PMID: 26620667.

(39) Mortensen, J. J.; Hansen, L. B.; Jacobsen, K. W. *Phys. Rev. B* **2005**, *71*, 035109.

(40) Enkovaara, J. et al. *Journal of Physics: Condensed Matter* **2010**, *22*, 253202.

(41) Yan, J.; Mortensen, J. J.; Jacobsen, K. W.; Thygesen, K. S. *Phys. Rev. B* **2011**, *83*, 245122.

(42) Bahn, S. R.; Jacobsen, K. W. *Comput. Sci. Eng.* **2002**, *4*, 56–66.

(43) Perdew, J. P.; Burke, K.; Ernzerhof, M. *Phys. Rev. Lett.* **1996**, *77*, 3865–3868.

(44) Hu, Z.; Metiu, H. *The Journal of Physical Chemistry C* **2011**, *115*, 5841–5845.

(45) Long, R.; English, N. J. *Molecular Simulation* **2010**, *36*, 618–632.

(46) Burdett, J. K.; Hughbanks, T.; Miller, G. J.; Richardson, J. W.; Smith, J. V. *Journal of the American Chemical Society* **1987**, *109*, 3639–3646.

(47) Lazzeri, M.; Vittadini, A.; Selloni, A. *Phys. Rev. B* **2001**, *63*, 155409.

(48) Esch, T. R.; Gadaczek, I.; Bredow, T. *Applied Surface Science* **2014**, *288*, 275 – 287.

(49) Bourikas, K.; Kordulis, C.; Lycourghiotis, A. *Chemical Reviews* **2014**, *114*, 9754–9823, PMID: 25253646.

(50) Bardo, R. D. *The Journal of Physical Chemistry* **1982**, *86*, 4658–4659.

(51) Ünal, H.; Gülseren, O. b. u.; Ellialtıoğlu, i. m. c.; Mete, E. *Phys. Rev. B* **2014**, *89*, 205127.

(52) Zhuomao, Z.; Baoan, B.; Haifeng, S. *Journal of Semiconductors* **2015**, *36*, 102003.

(53) Li, H.; Guo, Y.; Robertson, J. *The Journal of Physical Chemistry C* **2015**, *119*, 18160–18166.

(54) Maeda, K.; Domen, K. *The Journal of Physical Chemistry C* **2007**, *111*, 7851–7861.

(55) Shockley, W.; Read, W. T. *Phys. Rev.* **1952**, *87*, 835–842.

(56) Hall, R. N. *Phys. Rev.* **1952**, *87*, 387–387.

(57) Walter, M.; Hkkinen, H.; Lehtovaara, L.; Puska, M.; Enkovaara, J.; Rostgaard, C.; Mortensen, J. J. *The Journal of Chemical Physics* **2008**, *128*, 244101.

(58) Castelli, I. E.; Pandey, M.; Thygesen, K. S.; Jacobsen, K. W. *Phys. Rev. B* **2015**, *91*, 165309.